Longevity increase of an impregnated Ni/CeO$_2$-Al$_2$O$_3$ dry reforming catalyst by indium

Anita Horváth [a,*], Miklós Németh [a], Andrea Beck [a], György Sáfrán [b], Valeria La Parola [c], Leonarda Francesca Liotta [c], Gregor Žerjav [d], Matevž Roškarič [d], Albin Pintar [d]

[a] Centre for Energy Research, Institute for Energy Security and Environmental Safety, Department of Surface Chemistry and Catalysis, Konkoly-Thege M. street 29–33, H-1121 Budapest, Hungary
[b] Centre for Energy Research, Institute of Technical Physics and Materials Science, Thin Film Physics Department, Konkoly-Thege M. street 29–33, H-1121 Budapest, Hungary
[c] Institute for the Study of Nanostructured Materials, National Research Council (ISMN -CNR), Via Ugo La Malfa 153, 90146 Palermo, Italy
[d] National Institute of Chemistry, Department of Inorganic Chemistry and Technology, Hajdrihova 19, SI-1001 Ljubljana, Slovenia

ARTICLE INFO

ABSTRACT

The catalytic and structural changes due to the presence of 0.25 wt% indium on a 3% Ni/CeO$_2$-Al$_2$O$_3$ catalyst prepared by impregnation method were investigated. Catalyst characterizations by XRD, TPR, XPS, TEM and DRIFTS (in presence of CO/CO$_2$/CH$_4$ +CO$_2$) were carried out. In the short (6 h) catalytic methane dry reforming tests at 650 °C both samples were stable, produced essentially no carbon, but indium lowered the activity. In the 4 day longevity tests at 675 °C, stable activity was achieved by the In-promoted catalyst in contrast with the continuous deactivation of the unpromoted Ni sample due to coking and sintering. Indium, partially alloyed with nickel, could better keep nickel in metallic state, and the increased CO$_2$ activation ability, the intimate Ni(In)-CeO$_2$ interface inside the support pores resulted in practically no coking.

1. Introduction

Recently it is generally accepted that the greenhouse gas emissions such as CO$_2$ and methane must be reduced because of their harmful effect on the climate. The always increasing energy demand should be satisfied rather by renewable energy carriers instead of combustion of fossil fuels. However, the available large reserves of relatively cheap methane could be utilized on environmentally more friendly way as chemical feedstock by its transformation to valuable products. Methane reforming by CO$_2$ (CH$_4$ +CO$_2$ ⇌ 2CO+2 H$_2$, dry reforming of methane, DRM) producing synthesis gas is an attractive option since it does not form CO$_2$ but converts and link it up with the synthesis chain of value added chemicals. For exploitation of CO$_2$ containing natural gas and biogas the DRM can be a direct way [1]. If the energy need of the highly endothermic process is provided by electricity from renewable energy it is even more advantageous; moreover, it could be an energy storage alternative of fluctuating solar and wind derived electricity, since the further processing of synthesis gas, the CO hydrogenation is exothermic [2].

DRM is an equilibrium reaction and due to its high positive enthalpy

(ΔH$_{298}$ K=247 kJ mol^{-1}) it requires high reaction temperature, above 500–600 °C. Proper catalysts can accelerate and more importantly drive the reaction in the intended direction depending on the reaction temperature, because several thermodynamically allowed equilibrium reactions can occur beside DRM. The most important ones are the methane decomposition (CH$_4$ ⇌ C+2 H$_2$), Boudouard reaction (2CO ⇌ C+CO$_2$), and reverse water gas shift reaction (RWGS, CO$_2$ +H$_2$ ⇌ CO+H$_2$O), that should be limited kinetically to reduce unwanted side products.The former two are the worst ones deactivating the catalyst and fouling the reactor by the carbon formed [3], while the third one reduces the H$_2$/CO product ratio. Other side reactions may be advantageous, as coke gasification (C+H$_2$O ⇌ CO +H$_2$) helping to remove carbon, and methane steam reforming (SRM, CH$_4$ +H$_2$O ⇌ CO+ 3 H$_2$) increasing the H$_2$/CO.

The low stability due to coking (especially in case of the most economical Ni based catalysts) [4] and sintering of the active phases are the most important problems of the catalytic DRM hindering its industrialization. A recent review nicely summarizes the most important synthetic approaches, the advances and the perspectives of nickel-based catalysts for dry reforming [5]. Within the tremendous DRM literature, the photo thermal or microwave-assisted thermal catalytic solutions can

be considered as hot topics [6,7].

Ni is highly active in CH_4 dissociation to CH_x (x = 0–3) and adsorbed H, but the accumulating inactive carbonaceous deposits can block the site or Ni-carbide may form, which is the potential source of graphitic carbon nanotube/fiber formation. To avoid this, the availability of oxidizing surface O or OH species derived from CO_2 activation should be provided. Beside the metallic sites, the supporting or promoting oxides via their basic sites or oxygen vacancies can adsorb and activate CO_2, and the metal/oxide interface is the most efficient for the reaction resulting CO and H_2 in such cases [8]. The active metal modification by a second metal may promote the reaction via alloying and tuning the reactant activation ability or reducing the carbide formation or CO disproportionation leading to coke. The optimal bimetallic alloy composition may be a key factor as was declared for example for NiCu alloy catalysts, when a proper quantity of Cu promoted CO_2 activation and enhanced the transformation of CH_x into syngas on Ni atoms [9]. Moreover, confinement of the optimal NiCu alloy composition within nanosize SiO_x spheres could further improve DRM properties and catalyst stability [10].

Earlier highly impeded coking of indium promoted Ni/SiO_2 catalyst with Ni/In = 3 at. ratio was demonstrated in DRM [11]. This effect was explained by the role of indium as nickel modifier via alloying and hindering the methane decomposition, increasing hydrogen retention on the surface [12] and reducing CO dissociation [13]. On the other side, it was suggested that In oxidized by CO_2 or the by-product H_2O forms In_xO_y on NiIn particles, which acts as reducible oxide providing active oxygen for gasification of CH_x species [13]. Indium effect was investigated also on alumina and ceria-promoted alumina (8 wt% CeO_2) supported Ni with low In-concentration prepared by deposition precipitation method (Ni/In atomic ratio=24). [14] Very strong In-impact was observed to mitigate dramatically the carbon deposition on Ni/Al_2O_3 that otherwise resulted in reactor fouling in a short time. Surprisingly, the CeO_2 promotion in the Ni/CeO_2-Al_2O_3 was much less effective: it extended the catalyst lifetime, and reduced coking, but in much lower extent than the In promotion. The In addition resulted to the lowest carbon selectivity on $NiIn/CeO_2$-Al_2O_3 sample. The key importance of the interfaces between Ni and CeO_2 of high oxygen mobility is widely reported in the literature enhancing CO_2 activation and oxygen availability for the CH_x oxidation [15,16]. For example, the active nickel-ceria boundary can be formed with a special synthesis method within the confined space of a SiO_2 sphere: in this case the core promotes activity and reduces carbon deposition, and the shell hinders sintering [17].

It is known that the preparation mode and all the pretreatment steps may lead to different catalytic performance even in the case when the concentration of all the catalyst constituents is the same. We decided to produce new catalysts with different nanostructure and different Ni-In-CeO_2 interface by the simple impregnation method instead of the previously applied deposition-precipitation [14]. Our main aim was to improve the Ni-ceria interface in order to decrease coking by changing the preparation method and to see what a minuscule indium content can add to this specific situation. The catalytic properties in DRM process were correlated with structural properties characterized by X-ray diffraction (XRD), temperature programmed reduction (TPR), X-ray photoelectron spectroscopy (XPS), CO adsorption followed by diffuse reflectance infrared Fourier transform spectroscopy (CO-DRIFTS), transmission electron microscopy (TEM) and scanning TEM with energy dispersive spectroscopy (STEM-EDS) both in the fresh state and after DRM reactions. Additionally, in situ DRM reactions were investigated by DRIFTS. The spectacular effect of the preparation method was confirmed and much more stable catalysts with significantly reduced coking were obtained still keeping the superiority of the In-promoted version that was active for 4 days.

2. Experimental

2.1. Catalyst preparation

The CeO_2-Al_2O_3 support was prepared by incipient wetness impregnation of a commercial alumina support (Aldrich, SSA=175 m^2g^{-1}, V_p =0.27 cm^3g^{-1}, pore size 5.3 nm). The impregnation was carried out at room temperature by adding slowly and dropwise an aqueous solution containing the proper amount of cerium nitrate hexahydrate to get 7 wt% Ce on Al_2O_3. In order to have a complete and uniform impregnation, the total volume of the solution was slightly higher than the pore volume of alumina. After drying overnight at room temperature, the powder was calcined at 500 °C for 2 h. The Ni/CeO_2-Al_2O_3 and the $NiIn/CeO_2$-Al_2O_3 samples (denoted as Ni-CeAl and NiIn-CeAl, respectively) were prepared with impregnation/coimpregnation using nickel(II) nitrate hexahydrate, indium(III) chloride and the CeO_2-Al_2O_2 support. The nominal metal loadings were 3 wt% Ni and 0.25 wt% In (Ni/In molar ratio=24). The dried sample powders were calcined at 650 °C for 2 h. Before DRIFTS, TEM, XRD and XPS measurements, the calcined samples were reduced ex situ at 750 °C for 1 h in hydrogen (denoted as ex situ calcined/reduced state), while before DRM test in situ at the same temperature.

2.2. Catalyst characterization methods

The specific surface area and the pore volume of the mixed support and the Ni-CeAl and NiIn-CeAl samples were determined from N_2 adsorption–desorption isotherms at − 196 °C using a Micromeritics ASAP 2020 instrument. The specific surface area was calculated through the Brunauer–Emmett–Teller (BET) method applied to the adsorption curve in the standard pressure range 0.05–0.3 P/P_0. By analysis of the desorption curve, using the BJH method, the mean pore size was obtained. The total pore volume (V_p) was evaluated on the basis of the amount of nitrogen adsorbed at the relative pressure of 0.95.

The crystalline structures of the calcined and the calcined/reduced samples were determined by powder X-ray diffraction patterns (XRD), measured by a Bruker D 5000 diffractometer equipped with a Cu K_α anode and graphite monochromator. The data were recorded in a 2θ range of 20°− 80° with a step size of 0.05° and time per step of 5 s. The crystalline phases were analyzed by means of International Centre for Diffraction Data (ICDD) database.

Reduction properties of the calcined catalysts were determined by temperature programmed reduction (TPR) in 5% H_2/Ar (30 ml/min) up to 1000 °C with a 10 °C/min rate in a Micromeritics AutoChem 2910 instrument. About 0.1 g sample was pre-treated in 5% O_2/He (30 ml/min) at 350 °C for 30 min and cooled down in He prior to the TPR experiment.

Morphology of the calcined/reduced and the spent catalysts was investigated by Transmission Electron Microscopy (TEM) in TEM, HRTEM and HAADF modes by means of a FEI Titan Themis 200 kV spherical aberration (Cs) - corrected TEM with 0.09 nm HRTEM and 0.16 nm STEM resolution. Composition of the samples was measured by STEM-EDS and elemental maps were obtained by spectrum imaging with 4 Thermofischer "Super X G1" EDS detectors built in the microscope.

In situ diffuse reflectance infrared Fourier transform spectroscopy (DRIFTS) was applied to study the surface-adsorbed species in 1% CO/Ar, 2% CO_2/Ar and in a 50% CH_4: 50% CO_2 DRM mixture at chosen temperatures in a Nicolet iS50 infrared spectrometer equipped with a Specac DRIFTS accessory and environmental chamber heatable up to 500 °C. All experiments started with an in situ reduction of the ex situ at 750 °C reduced sample: the catalyst in the cell was reduced in 5% H_2/Ar at 500 °C for 30 min, and then it was cooled down to room temperature in the same gas flow. CO-DRIFTS experiments were carried out in 1% CO/Ar at room temperature and after the temperature programmed desorption in 5% H_2/Ar flow that perfectly cleaned the surface again at

300 °C. CO$_2$-DRIFTS experiments at 300 °C were done on a freshly reduced sample, while DRM-DRIFTS experiments were performed after a subsequent regenerating treatment in 5% H$_2$/Ar at 500 °C/30 min followed by a cooling step to 300 °C. These DRM experiments were carried out in a temperature ramped mode from 300 °C to 500 °C range followed by a 30 min isothermal hold at 500 °C and a final cooling step to 300 °C still in the CH$_4$-CO$_2$ mixture. All spectra shown here were corrected with the appropriate spectrum (background) taken just before the admission of the actual reactant.

Surface compositions of the samples were determined by X-Ray photoelectron spectroscopy (XPS) in a KRATOS XSAM 800 instrument. The samples were analyzed by using an unmonochromatized Al K-alpha source (1486.6 eV). The Al 2p binding energy from the alumina support set at 74.4 eV was used as reference for charge compensation. The ex situ calcined/reduced samples were measured directly and then again after an in-situ reduction at 500 °C in H$_2$ using the instrument's atmospheric pretreatment chamber. Because of the low amount of cerium and the overlapping of Ce 3d$_{5/2}$ with the Ni 2p$_{1/2}$ peaks, for evaluation of Ce^{3+} amount the data treatment of Pardo and his co-workers [18] was used. Shortly, the Ce(IV)% of cerium is estimated by calculating the attenuation of the u‴ component at 917 eV with respect to the total area of the Ce 3d peak after subtracting the Ni 2p$_{1/2}$ contribution [9]. The Ce^{3+} content in % was calculated according to Eq. (1):

$$Ce(III)\% = 100 - Ce(IV)\% = 100 - u''' \% /14 \times 100 \qquad (1)$$

where u‴ is the area fraction of the peak at 917 eV. When there is only Ce^{4+} present in the sample (as in pure CeO$_2$), the u‴ peak is 14% of the total area of the Ce 3d multiplet.

2.3. Catalytic studies

2.3.1. Short DRM tests at 650 °C followed by the temperature programmed oxidation of coke

The 6-h catalytic runs were done in a fixed-bed quartz reactor of 4 mm inner diameter, where the thermocouple for temperature control was fixed to the outer surface of the quartz tube. 20 mg of a calcined catalyst with 70 mg of diluting quartz beads were placed into the reactor and reduced in 30 ml/min 90% H$_2$/Ar at 750 °C (ramp rate was 10 °C/min) for 1 h. Subsequently, the sample was cooled down to 650 °C in 10 min under He purge, then the equimolar CH$_4$:CO$_2$:Ar = 49.5:49.5:1 reactant mixture with 70 ml/min flow rate (210 L/h/g$_{cat}$) was switched. Reaction was allowed to proceed for 6 h. A quadrupole Pfeiffer Prisma spectrometer was used for gas analysis, and the quantification of mass flow rates of H$_2$, CH$_4$, CO and CO$_2$ components were done in the way described in ref [11].

Temperature programmed oxidation (TPO) measurements after cooling the sample in He to room temperature were done in 40 ml/min flow of O$_2$:He:Ar= 10:89:1 mixture with temperature ramp to 650 °C followed by a 30 min isothermal hold. The pre-calibrated CO$_2$ signal was used to quantify any carbon deposits.

2.3.2. Catalytic DRM longevity tests

These tests were performed using a Microactivity Reference reactor system (MA-Ref from PID Eng&Tech, Madrid, Spain) equipped with a quartz tubular reactor (inner diameter = 10 mm). A catalyst sample was placed in a fixed bed of 20 mg of well-mixed catalyst powder with 180 mg of diluting quartz beads and positioned on a flock of quartz wool in the reactor tube. The temperature was measured with a K-type thermocouple placed in the center of the catalyst bed. The catalyst was first degassed in N$_2$ stream (50 ml/min) at 200 °C and then reduced in situ in H$_2$ stream of 50 ml/min by heating from 200° to 750°C with a ramp of 10 °C/min. This was followed by an isothermal step at 750 °C for 1 h. The catalyst was then cooled to 675 °C in N$_2$ stream (50 ml/min). The CH$_4$-CO$_2$ DRM activity test was performed at the same temperature and atmospheric pressure with an undiluted and equimolar CH$_4$/CO$_2$

mixture (70 ml/min). The reactor outlet stream was passed through a heated transfer capillary (I.D.=0.16 cm at 200 °C) to the GC instrument (Agilent Technologies, model 7890 A) equipped with Poraplot Q and Molesieve 5 A capillary columns, in which quantitative analysis of gases exiting the reactor outlet was recorded every 26 min. After the test, the deposited carbon was measured by TPO experiment in 40 ml/min O$_2$: He:Ar= 10:89:1 mixture with 10 °C/min ramp rate to 650 °C followed by a 30 min isothermal hold. The pre-calibrated CO$_2$ signal was used to quantify any carbon deposits as before.

3. Results and discussion

3.1. Structural results of N$_2$ adsorption, XRD, TPR and TEM

Compared to the original BET of alumina support, the Ce-modification induced a decrease in the surface area from 174 m^2/g to 129 m^2/g, but the introduction of nickel component caused no further decrease of pore volume and pore diameter data (it was fixed at 0.2 cm^3/g and 5.4 nm, respectively). This means, that the cerium precursor was actually introduced into the pores of the alumina, which also led to a shrinkage of the original pore volume (beside of the calcination treatment itself).

Reduction properties of the calcined samples were investigated by Temperature Programmed Reduction (TPR) in 5% H$_2$/Ar up to 1000 °C, and the obtained results are shown in Fig. 1 and collected in Table 1. The TPR profiles of the two samples are very similar: a small weak peak was detected at around 300 °C and a large one just below 800 °C. Indium introduction caused a decrease in the temperatures of peak maxima of both peaks. The low temperature peak may be linked to the reduction of surface ceria species [19] or some easily reducible NiO-CeO$_x$(-InO$_y$) compound on the alumina surface. Most NiO species are definitely in very strong interaction with the CeO$_2$-Al$_2$O$_3$ support, as the majority of NiO started to get reduced above 600 °C. It is known that TPR peak at temperatures of 750 °C or above is attributed to surface or the bulk reduction of NiAl$_2$O$_4$ [20,21]. The small difference in the peak maxima in favor of NiIn-CeAl sample might mean that indium promotes the reduction of the NiO-CeO$_2$-Al$_2$O$_3$ mixed solid solution. The total H$_2$ consumption is listed in Table 1 in terms of mmol H$_2$/g$_{cat}$. The expected hydrogen consumption for the total reduction of NiO to Ni is 0.51 mmol/g while the reduction of In$_2$O$_3$ to In would count for 0.02 mmol/g. The total consumption is higher because of the concomitant reduction of ceria influencing the H$_2$ uptake. Nevertheless, it appears that the
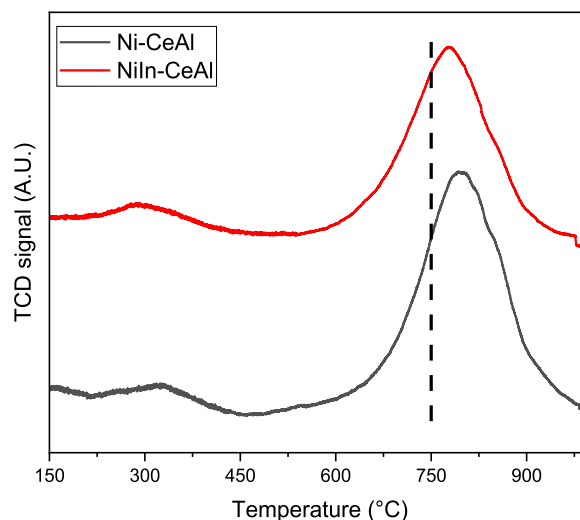

Fig. 1. TPR profiles of the calcined catalyst samples obtained under 5% H$_2$/Ar flow. (The broken line signs the reduction temperature applied prior to the catalytic reaction.)

Table 1
Quantification results of the TPR spectra.

Samples	T1 (°C)	H$_2$ consumption (mmolg^{-1})	T2 (°C)	H$_2$ consumption (mmolg^{-1})	Total H$_2$ consumption (mmolg^{-1})
Ni-CeAl	323	0.06	792	0.53	0.59
NiIn-CeAl	302	0.08	777	0.62	0.70

presence of indium promotes the reduction of ceria increasing the total hydrogen consumption [22,23], but NiO remains in a very strong interaction with the mixed oxide anyway. We should note that the 750 °C reduction treatment applied before the catalytic reactions could surely not bring all the nickel-oxide into a metallic state.

Fig. 2a and b show the XRD patterns of the calcined and calcined/reduced catalysts together with the reference patterns of NiO (00–044–1159) and NiAl$_2$O$_4$ (00–001–1299) and the pattern of bare support (both Al$_2$O$_3$ and CeAl). Nothing but the 7 nm sized crystallites of cubic ceria could be identified beside alumina in all calcined samples.

It was not possible to distinguish between segregated NiO or NiAl$_2$O$_4$ because the main diffraction peaks would overlap with their diffraction peaks of alumina and CeO$_2$. After the ex situ reduction treatment, peaks attributed to metallic nickel at 44.5 and 51.9 2theta appeared for both samples. Based on thesepeaks relative to the support at 47.5 and 56.4 2theta, the contribution of ceria appears less intense probably due to the partial reduction of ceria during the pretreatment procedure. A very
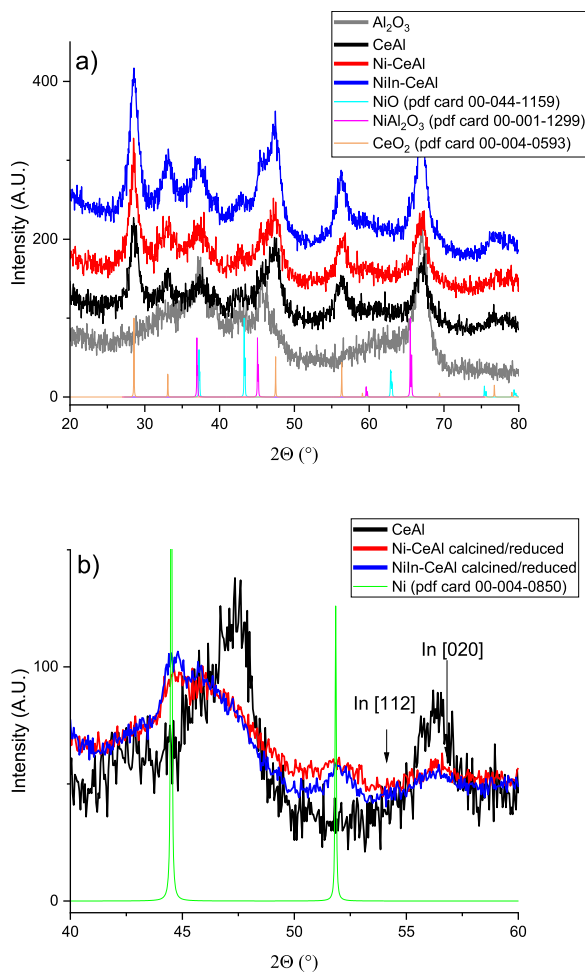
Fig. 2. XRD pattern of: a) calcined Al$_2$O$_3$; CeAl support; Ni-CeAl and NiIn-CeAl samples along with reference pattern of NiO and NiAl$_2$O$_3$ and b) reduced CeAl, Ni-CeAl and NiIn-CeAl and reference curve of metallic Ni.

rough estimation of the nickel crystallite size based on the Ni (200) peak resulted in 4.6 nm for Ni-CeAl and around 8.9 nm for NiIn-CeAl. It is worth to note that these values are affected by large errors because of the short range of the measurement and the overlapping of the peaks, so we highlight just that larger crystallite size is found in the case of the bimetallic sample. This general trend is confirmed also by the analysis of the Ni (111) peaks, which suffer of a higher error, and give different size values (3.2 nm for Ni-CeAl and 3.9 nm for NiIn-CeAl), but maintain the same trend. For the same reason, it is not possible to speculate about the formation of any alloy between nickel and indium. Moreover, no features attributable to segregated metallic indium were seen (54.4 2theta and 56.5 2theta for In [112] and In [020]) [24].

The catalyst morphology was further investigated by TEM/HRTEM analysis (see Fig. 3a-f). The EDS elemental mapping could provide some information about the distribution of Ni, Ce and In after the ex situ calcination/reduction treatment (calcination at 650 °C/reduction at 750 °C). In general, Ni particles were really hard to spot based on the usual contrast method, as the heavy ceria might also give darker spots if concentrated. On the monometallic Ni sample the presence of larger particles was suspected based on TEM image of Fig. 3a, and ascertained by HAADF and STEM-EDS images (Fig. 3b and c), but such larger particles with 10 nm sized Ni were not spot at other places. In addition, the STEM-EDS shown in Fig. 3c proves that ceria is nicely distributed in the sample. Ni in the bimetallic sample (Fig. 3d) was highly dispersed, as only elemental mapping could prove the location of small Ni(In) particles with particle sizes less than 10 nm as suspected based on the HAADF image and the elemental mapping of the same area (Fig. 3e and f). Indium signal was detected everywhere, also at places where Ni particle-shaped entities were not present, and the Ni/In ratio could be reasonably determined only for such large areas but not for individual Ni particles (Ni/In=10 was measured here). The low loading and the rather dispersed state of indium resulted in a higher uncertainty when defining the location of indium, but based on the In map, we would suggest that indium is associated with both the support and the nickel particles and it is not enriched in/on nickel as was observed with the same loading in the case of the deposition precipitation synthesis method [14].

TEM analysis revealed that the ceria modifier was uniformly distributed over the alumina. The average nickel particle size could not be given, but a rough estimate based on the elemental maps gives d< 5 nm for both samples with some larger exceptions for the Ni-CeAl catalyst. As for indium, such an enrichment of indium in the nickel particles as seen in our previous publication for DP prepared samples [14] cannot be ascertained. Instead, a fine distribution of indium can be assumed, which does not exclude the existence of a NiIn alloy.

3.2. XPS characterization results

The XPS spectra obtained over the ex situ calcined/reduced samples and after the in situ reduction are shown in Fig. S1 and the derived data are listed in Table 2.

The in situ reduction at 500 °C in the XPS pretreatment chamber must have ensured the same state of the catalysts as was present after the ex situ 750 °C reduction. The extremely low nickel signal intensities detected over both samples (nominal Al/Ni$_{bulk}$ =35) suggested that metal particles are hidden inside the pores of the support or covered by CeO$_2$-Al$_2$O$_3$ moieties because of the very strong metal-support interaction proved by TPR. The metallic portion of nickel is higher (80%) in the case of indium-promotion. This suggests that indium is alloyed with nickel or it greatly influences the reduction property of nickel-oxide. As for the quantification of surface ceria concentration, we should be aware that ceria peaks in the 3 d region overlap with the Ni 2p$_{1/2}$ peaks. Thus, instead of the classic fitting method of Burrough [25], we used the method of Pardo [18] for the determination of Ce^{3+} amount as described in our earlier work [14]. The surface ceria concentration was the same for both samples, but the Ce^{3+} contribution was a bit higher in Ni-CeAl, while proportion of oxidic nickel was more – in complete agreement
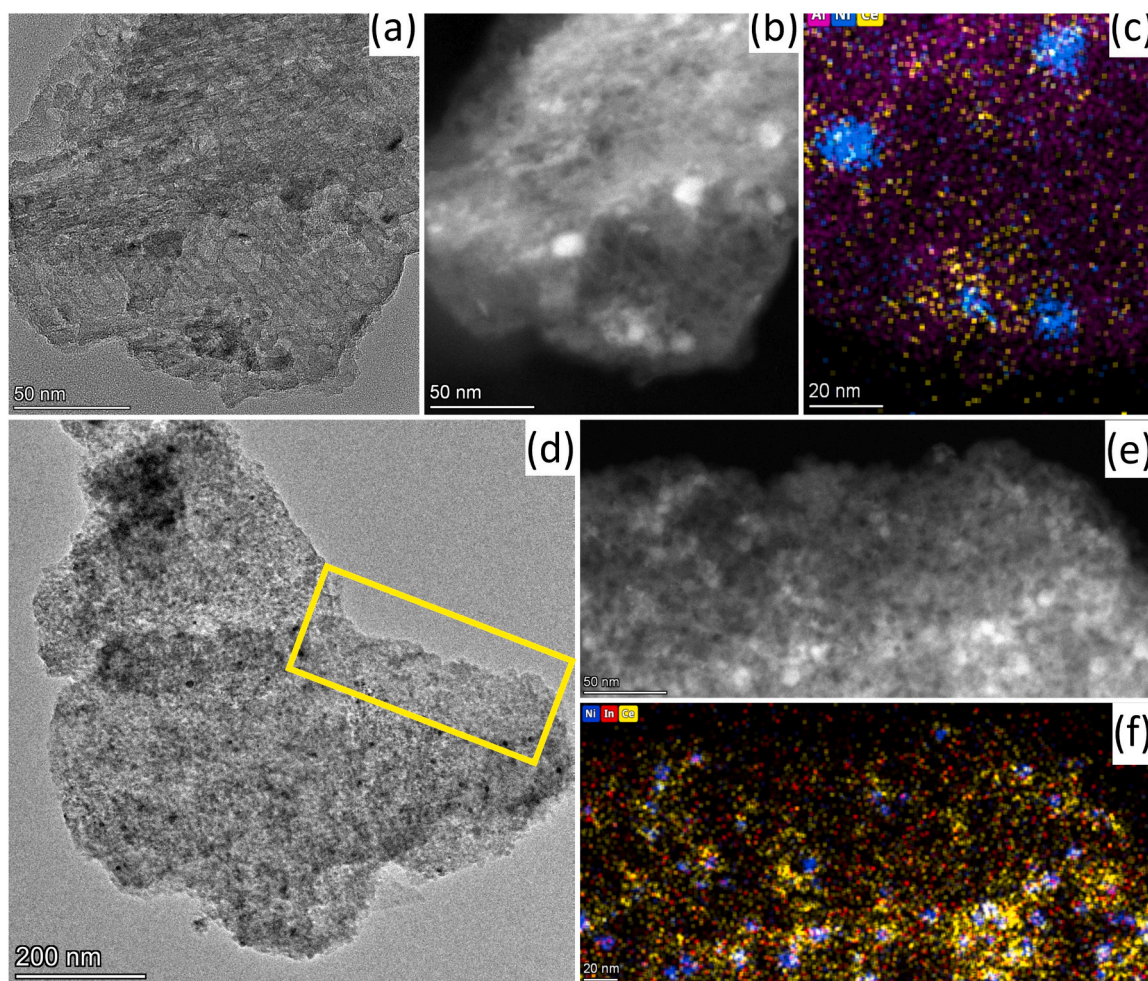
Fig. 3. TEM results of the calcined/reduced catalysts. a) TEM of Ni-CeAl sample; b) HAADF image of the same area; c) EDS elemental maps of Al, Ni, Ce obtained over the same area; d) TEM of NiIn-CeAl; e) HAADF image of the signed area; f) EDS elemental maps of Ni, In, Ce obtained over the same area.

Table 2

XPS results on calcined/reduced catalysts: surface composition data and relative amount of metallic nickel and Ce^{3+} sites.

Sample name	Atomic ratios				Ce^{3+}	Ni^0
	Al/Ni	Al/Ce	Al/In	Ni/In	(%)[a]	(%)[b]
Ni-CeAl	55.6	16.16	-	-	65	63.1
NiIn-CeAl	87.9	16.07	633.2	7.2	59	79.2

[a] percentage of Ce^{3+} in the total Ce content detectable by XPS
[b] percentage of metallic Ni^0 in the total Ni content detectable by XPS

with the TPR results. If more Ni^{2+} ions remain occluded inside the ceria structure, this can cause more oxygen vacancy and higher concentration of Ce^{3+}. The BE of indium 3 $d_{5/2}$ shifted with 0.4 eV upon the in situ reduction treatment (from 444.7 eV to 444.3 eV, spectrum not shown) demonstrating that part of indium became metallic (alloyed with nickel). The surface Ni/In was 7.2 in the reduced sample, which indicates that In was better enriched and more dispersed close to the up-most surface of the catalyst than Ni, because the nominal bulk Ni/In value is 24. These XPS results signify that indium enhances the amount of metallic nickel via its intimate contact or alloy formation with Ni and reduces the surface concentration of Ce^{3+}.

3.3. Interaction of CO and CO₂ with the catalysts investigated by DRIFTS

The changes in the vibration frequency of the adsorbed CO molecules can deliver useful information about the particle size, surface structure and electron density of adsorbing metal [26]. The gas phase CO vibrations are located between 2100 and 2200 cm^{-1}, while CO molecules bonded to a surface nickel atom through the carbon end give bands above 2000 cm^{-1} (linear adsorption geometry on dense facets at around 2050 cm^{-1} [27,28]), and CO bonded to 2 or 3 Ni atoms results in IR bands below 2000 cm^{-1} in the bridged CO region [29,30]. CO bonded to kinks, adatoms and edges or the linear di and tri carbonyls are detected at higher wavelength of the linear CO region [29,30].

First, the data of CO chemisorption at room temperature followed by the temperature ramped desorption experiments will be evaluated. The red curves of Fig. 4a and b show the spectra taken in 1% CO/Ar mixture at room temperature over Ni-CeAl and NiIn-CeAl samples. The main difference beside the higher CO band intensity of NiIn-CeAl catalyst is the higher linear/bridge CO band ratio. This was already reported for our previous In-containing Ni samples and described as the surface dilution effect of alloying indium component (the number of Ni-Ni neighbors is less and so the possibility to form bridged CO species is less as well). Another important feature to spot is the red shift of the linear CO bands related to those registered on the monometallic Ni-CeAl (2086→2062 cm^{-1} for CO bonded to highly undercoordinated Ni sites, 2050→2030 cm^{-1} for CO adsorbed on dense facets) as it was already noticed for the samples prepared by deposition precipitation. This is assignable to the electronic and diluting effect of indium neighbors of Ni sites increasing their electron density and reducing the dipole-dipole interaction between adsorbed CO molecules [14]. The desorption of adsorbed CO in the presence of 5% H₂/Ar flow is also shown in Fig. 4.
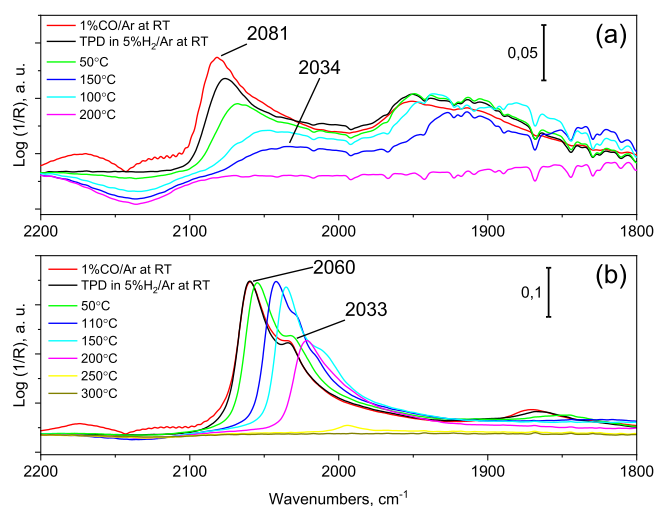
Fig. 4. DRIFT spectra of adsorbed CO at room temperature in 1% CO/Ar (red curves) and the desorption spectra taken in 5% H_2/Ar at 25 °C and then during temperature increase over a) Ni-CeAl and b) NiIn-CeAl sample.

The pure Ni sample behaved as expected: CO bands continuously decreased in intensity and redshifted due to the decreased dipole-dipole interaction at lower coverage ($2081 \rightarrow 2034, 1950, 1920, 1835$ cm^{-1}), but above 150 °C no adsorbed CO band was observed. In contrast, the CO band area of the bimetallic sample did not change up to 150 °C, only shifted strongly towards the lower wavenumbers from 2060 cm^{-1} to 2035 cm^{-1}, then a big drop was observed at 200 °C, but a final small CO band at 1993 cm^{-1} was still visible reaching 250 °C. The higher stability and the strong redshift at unchanged coverage of adsorbed CO is obvious. This undoubtedly proves the existence of surface or bulk NiIn alloy that changes its composition, electron density or morphology during temperature increase and acts against the normal desorption tendency (very strong redshift). (Note that indium should be highly mobile on/within nickel as its bulk melting point is 156.6 °C.) Beside H_2O, no other surface-bonded species, carbonate or formate were observed during these experiments (the corresponding region is not shown).
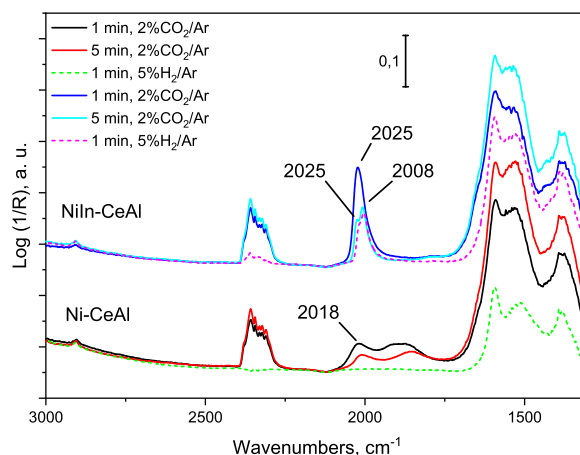
The nature of Ni atoms in the neighborhood of indium atoms was further investigated with CO chemisorption carried out at 300 °C. Fig. 5 collects the spectra under 1%CO/Ar flow at 1 min and a few min after introducing the gas onto the catalysts. (Note that 5% H_2/Ar was
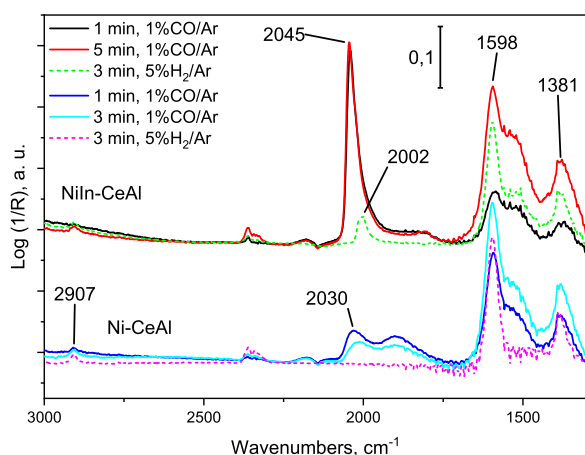
switched to 1%CO/Ar at 0 min of the experiment). Again, as at room temperature, higher CO band intensity was detected over the bimetallic sample, almost exclusively in the linear CO band region at 2045 cm^{-1}, and the band intensity was unchanged during the first 5 min. In contrast, both linear (at 2030 cm^{-1}) and bridge CO bands over Ni-CeAl decreased fast. This means, CO decomposition happened on the H_2 covered pure Ni, poisoning the adsorption sites. Over both samples formate bands (2907, 1598, 1391, 1381 cm^{-1}) were building up continuously as CO interacted with the support, which is expected at this temperature. Upon the 3 min 5% H_2/Ar flush after the CO adsorption, there was still adsorbed CO visible on NiIn-CeAl catalyst at 2002 cm^{-1}, some formate and a little carbonate species as well. In the case of Ni-CeAl, no adsorbed CO but the same sized formate bands were observed. From the small changes in the intensity of the gas-phase CO_2 band around 2350 cm^{-1} no conclusions could be deduced, since the sample compartment of the spectrometer where the DRIFTS environmental chamber located is not closed. This means, gas phase CO_2 signal can be changed due to the change of the gas composition inside the IR cell or simply in the ambient atmosphere. Due to these restrictions we are not able to tell how the CO_2 was formed on Ni-CeAl under the H_2-flush, if the CO disproportionated, or the formates decomposed, or the CeO_2 component oxidized the adsorbed CO, etc. On the other side, we cannot tell if a lower CO_2 signal in the case of the bimetallic sample is whether connected to the increased RWGS activity of indium component.

The same temperature of 300 °C was chosen to investigate the interaction of CO_2 with the H_2-covered catalysts as to mimic a RWGS reaction and detect CO_2 activation steps depending on the presence or absence of NiIn alloy. Fig. 6 depicts spectra grouped in two for the two samples. The lower curves are those obtained in the presence of 2% CO_2/Ar at 1 and 5 min of exposure and then after 1 min flush in the 5% H_2/Ar stream over the Ni-CeAl sample. The CO_2 obviously dissociated and the resulting CO was adsorbed on the available Ni sites but the carbonyl band intensity decreased within the 1–5 min interval. This again shows the surface poisoning process by surface nickel oxidation or carbon formation. The maximum intensity of carbonyl band (with a linear component at 2018 cm^{-1}) was the same as in the presence of 1% CO/Ar at the same, 1 min exposure time. The places of CO_2 dissociation beside the Ni surface are the oxygen vacancies of the ceria additive. At lower wavenumbers, support-bonded carbonates and formates were also detected. These latter are due to the initial reduction of carbonates and the reaction of $CO_{ads} + OH_{support}$. The spectra of the bimetallic catalyst shown on the upper part of the figure reflect that CO_2 activation resulted in adsorbed CO too, and after 5 min the intensity of Ni-adsorbed carbonyl bands was lower as well (in contrast to the CO@300 °C

Fig. 5. DRIFT spectra of adsorbed species in 1% CO/Ar at 1 min and 5 or 3 min of exposure at 300 °C and the desorption spectra (dashed lines) taken in 5% H_2/Ar 3 min after the gas switch over NiIn-CeAl sample (upper group) and Ni-CeAl (lower group).

Fig. 6. DRIFT spectra of adsorbed species in 2% CO_2/Ar at 1 and 5 min of exposure at 300 °C and the desorption spectra (dashed lines) taken in 5% H_2/Ar 1 min after the gas switch over NiIn-CeAl (upper group) and Ni-CeAl (lower group) samples.

experiments on this sample). Moreover, the original band with a maximum at 2025 cm^{-1} splits into 2 components (at 2025 and 2008 cm^{-1}). We saw in the CO-DRIFTS@ 300 °C experiments above that CO apparently does not dissociate under the same conditions over NiIn-CeAl. Thus, the present intensity decrease must be caused by the CO_2 activation step resulting CO+O close to or on the metal sites. The mobile oxygen must reach Ni easily, to cause continuous oxidation and decline CO adsorption ability. This means that CO_2 activation results in facile oxidation of metallic sites and so this activation happens close to the metal at the metal/support interface. The carbonate region of this sample is very similar in intensity to that of Ni-CeAl catalyst, thus, the pure CeO_2-Al_2O_3 part of the support (not contacting or far from metal particles) has the same acid-base properties. If we compare the spectra after 1 min of 5% H_2/Ar flush, the monometallic sample has only adsorbed carbonates and formate bands, while the bimetallic one due to the higher stability and concentration of chemisorbed CO species, still has the same 2 component carbonyl band discernible beside the more intense carbonate-formate bands.

Shortly, the main difference between the samples is that CO does not dissociate on NiIn while it does on pure Ni as this was proven on a NiIn/SiO_2 catalyst but with much higher, 2% In loading by pulse CO experiments followed by QMS [13].

3.4. Interaction of a stoichiometric CO_2-CH_4 DRM mixture with the catalysts investigated by DRIFTS

DRIFTS experiments were carried out in the presence of a methane dry reforming mixture introduced onto the reduced catalyst at 300 °C, ramped to 500 °C, kept there for 30 min and cooled to 300 °C under the reactant mixture. Chosen spectra in Fig. 7 show the main differences observed during these measurements. Beside gas-phase CO_2 and CH_4 bands, chemisorbed CO, carbonates and formates could be distinguished on both samples. At lower temperatures (bridged) bidentate carbonates (1650, 1350 cm^{-1}) were also present, but at 500 °C only monodentate carbonates (1530, 1360 cm^{-1}) and formate species (1595 cm^{-1}) were stable [31] on both samples. In a diluted H_2 stream, the bridged carbonates transform to formates on both samples. This similarity means again that the presence of In promoter in the support oxide cannot be detected by means of DRIFTS method. The In loading is extremely low, and some part of it seems to be alloyed with nickel, the remaining one might cause variance in the number of extrinsic oxygen vacancies, but the other than spectator role of carbonates and formates could not be proven in the present case via
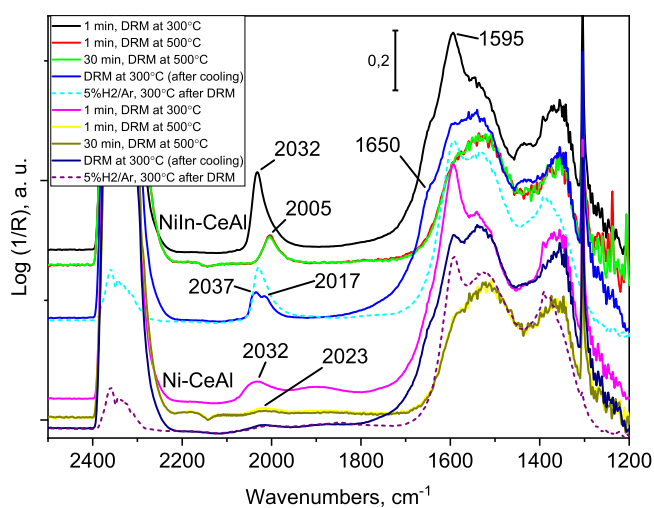
DRIFTS.

If we compare the metal-bonded carbonyl regions, the following statements can be drawn. The lower stack of curves belongs to the Ni-CeAl sample in Fig. 7. The usual broad band with linear CO at 2032 cm^{-1} and bridged ones with a maximum at 1904 cm^{-1} at 300 °C was detected that lost from their intensities, with the redshift of the linear component to 2023 cm^{-1} by reaching and staying at 500 °C for 30 min. The gas-phase CO product of the reaction was easily spot (higher than on NiIn-CeAl sample), revealing the good activity of this sample. Going down again to 300 °C in the reaction mixture, the weak carbonyl band intensity and position remained basically the same. H_2 flush (dashed line) caused a slight decrease in the tiny CO band intensity and removed the bridged carbonates.

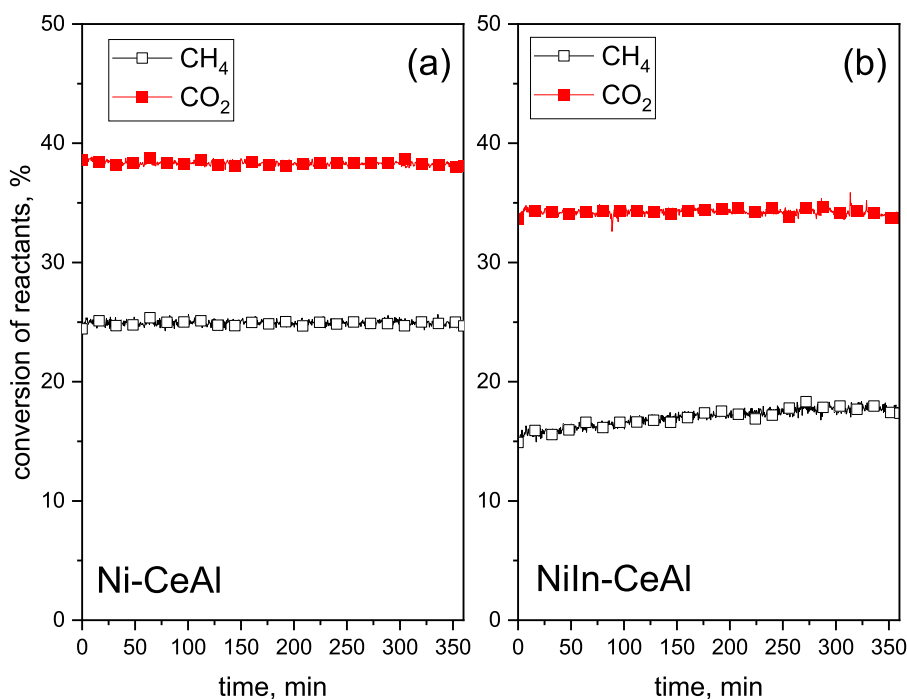As for the bimetallic counterpart shown on the upper part of Fig. 7, the strong linear CO band at 2032 cm^{-1} (red shifted compared to that observed in 1% CO/Ar in Fig. 5, due to the lower CO coverage in the DRM mixture) weakened and shifted to 2005 cm^{-1} by 500 °C, remained the same for 30 min and by cooling to 300 °C, blue shifted and split into 2 components at 2037 and 2017 cm^{-1} without losing anything from the intensity measured at 500 °C. This suggests that a kind of oxidation happens and InO_xH_y might form causing NiIn surface segregation and the split of carbonyl peak, as was already detected with our In-rich NiIn/SiO_2 sample [13]. Last, when the gas was switched to a 5% H_2/Ar mixture, the CO band intensity increased and the 2 components apparently merged into one with a maximum at 2030 cm^{-1}. Note that there was no CO source in the gas phase after the switch, so the increase of carbonyl band must be explained. In our opinion, the existing carbonates-formates could be decomposed and produce chemisorbed CO species on NiIn, or the H_2 caused the reduction of ceria and deliberated some oxygen or OH to react with CH_x on the metal sites resulting in adsorbed CO. This would suggest the existence of easily oxidizable CH_x species and the higher mobility of surface oxygen/OH that can be used for carbon removal on NiIn-CeAl. This is not valid for the monometallic Ni sample, viz., the reaction produces such a Ni state that is more active (see the larger CO gas bands at 500 °C than on the bimetallic sample), but CO cannot be produced by a sudden hydrogen contact of the spent surface. This might include the irreversibility of CH_4 dissociation into carbidic carbon over Ni. It is known that a marked weakening of the metal–CO bond can happen in the presence of surface carbon or carbide [29].

Based on these DRIFTS-DRM experiments, we would expect a higher catalytic activity of Ni-CeAl sample and a better coking-resistance of NiIn-CeAl in the catalytic tests in plug flow reactors. However, the temperature difference (500 °C of DRIFTS-DRM versus 650 or 675 °C) can cause large deviations from these expectations.

3.5. Catalytic activity and coking properties in dry reforming, analysis of spent catalysts

3.5.1. Results of the short catalytic tests at 650 °C

Two experimental setups were used for the catalytic tests differing greatly in reactor and temperature sensor's geometry and analysis method. In both cases, reduction pretreatment at 750 °C was performed and the sample was cooled in inert to the reaction temperature. The 6-h "short" tests were carried out with QMS product analysis method. Fig. 8 depicts the CH_4 and CO_2 conversion curves obtained during this short DRM test at 650 °C. We can see that Ni-CeAl is extremely stable thorough this TOS having CO_2 conversion (40%) much higher than CH_4 conversion (25%). The bimetallic sample was also highly stable, only both reactant conversions were lower. This lower activity was already observed in other In-promoted sample prepared by deposition precipitation synthesis method and it is due to the decreased CH_4 dissociation ability of the NiIn alloy [12–14]. The other simple explanation would be the lower dispersion, but this was not revealed neither by XPS nor by the CO-DRIFTS results of NiIn-CeAl. The increase of the ratio of CO_2/CH_4 conversions in favor of In-added sample reflects the increased RWGS

Fig. 7. DRIFT spectra of adsorbed species in CH_4:CO_2 = 50:50 DRM mixture and 1 min after switching to 5% H_2/Ar at the end of the experiments (dashed lines) over NiIn-CeAl (upper group) and Ni-CeAl (lower group) samples.

Fig. 8. Methane and CO_2 conversion curves during the short DRM test. H_2/CO ratio at the start of the reaction was 0.64 for Ni-CeAl and 0.53 for NiIn-CeAl. Conditions: after reduction at 750 °C/1 h cooling to T = 650 °C in He, then DRM with $CH_4:CO_2:Ar$ = 49.5:49.5:1 mixture, 210 L/h/$g_{cat.}$, TOS= 6 h.

activity induced by indium inclusion. It is known that ceria has signifi-cant WGS activity at moderate temperatures [32], but the RWGS activity can be even enhanced over In_2O_3-CeO_2 [33]. Thus, InO_xH_y at the Ni-support interface must also play a role in these processes. The water formed during RWGS may contribute to the surface carbon gasification and coke removal. Quantifying the deposited carbon by TPO experi-ments of the spent samples revealed almost no coking in both cases: 0.05 wt% C was detected on Ni-CeAl and 0.03 wt% C was measured on NiIn-CeAl.

Ceria modification of alumina in the present case was perfectly effective in preventing coke deposition that would be otherwise ex-pected on pure Al_2O_3 support. Due to the strong interaction between the metallic nickel and the oxidic components in the NiO-CeO_2-Al_2O_3 ma-trix, under this reaction conditions we got a stable catalyst. The indium promotion decreased the activity (since Ni is alloyed with In), but maintained the stability with the same, close to zero carbon deposition.

Next, TEM measurements were carried out to detect possible morphological changes on the spent samples. Fig. 9 testifies that in the compact structure of the catalyst, Ni particles are still hard to discover. This means that Ni remained nicely dispersed after 6 h of time on stream at 650 °C. The surely discernible Ni particles were measured and the result was 3 nm for Ni-CeAl and 3.7 nm for NiIn-CeAl, but reliable size distribution cannot be given based on the low number of particles. Fig. 9b shows the enlarged image of the circled area in Fig. 9a: the close contact of CeO_2 and a tiny Ni particle was captured. This proves that the 3 nm sized Ni and the 4 nm sized surface CeO_2 entities can work side by side over the large surface of Al_2O_3 making the Ni/CeO_2 interaction effective in fighting with coke deposition. The elemental Ni (and Al, Ce) mapping image in Fig. 9c helps to find the ~3.8 nm sized Ni particles that are almost invisible otherwise in a normal TEM image.

Fig. 9d and e depict the bimetallic spent catalyst, showing a TEM image and its corresponding STEM-EDS Ni, In, Ce elemental maps. Both the size of Ni(In) and the distribution of Ce compound are very similar to that of Ni-CeAl, which means that the differences observed in catalytic and DRIFTS experiments cannot be supported or denied by TEM. A Ni/ In= 17 ratio was obtained over the measured area here, which means that close to the nominal Ni/In ratio exists on such a small area.

3.5.2. Results of the 4 day-longevity catalytic tests at 675 °C

The 96 h longevity tests at 675 °C were performed in a different catalytic reactor consisting of a thinner catalyst bed in a wider quartz tube and a thermocouple inserted into the catalyst bed. These are important parameters to mention, and the only 25 °C difference in re-action temperature compared to the short tests might mean more in reality, as DRM is an endothermic reaction and so inside the catalyst bed the real temperature might have been a bit lower than 650 °C set by the thermocouple on the outer wall of the quartz reactor tube of short tests. Another difference was that the GC analysis used for quantification provided data only after the first 26 min of the reaction. This means that any rapid deactivation process upon contact with the reaction gas could not be noticed in this case.

Fig. 10 shows the conversion values obtained during these long-term tests. It is eye-catching that the Ni-CeAl sample (Fig. 10a) deactivated with a continuous decrease of both CO_2 and CH_4 conversions, although the first 6 h of this long term test would not suggest such deactivation tendency, because the conversion of both reactants was almost identical to the ones in the short term measurements. This is why the long term stability tests of catalyst samples are very precious and indispensably helpful when deciding which catalyst formulation has an eventual good property. Without carrying out such a long measurement, just based on the 6 h-experiment at 650 °C, one would vote for the nice activity and stability of unpromoted Ni-CeAl versus the less active NiIn-CeAl sample. The CO_2/CH_4 conversion ratio was 1.5 on Ni-CeAl, very similar to the result of short test, and so was the H_2/CO ratio (0.62). These two ratios signify that beside DRM, reverse water gas shift reaction (CO_2 +$H_2 \rightleftharpoons CO+H_2O$) occurs as well, whereas other reactions ($2CO \rightleftharpoons C+CO_2$, $CO+H_2 \rightleftharpoons C+H_2O$) that affect the H_2/CO ratio may have further influ-ence [34]. Moreover, it was reported that nickel ions in ceria lattice and highly dispersed NiO after reduction are responsible for the high yield of CO in RWGS at high temperature [35].

As for the performance of the bimetallic NiIn-CeAl sample shown in Fig. 10b, the starting conversions of both reactant were just a bit lower than on Ni-CeAl, but the activity remained nicely stable with only a slight deactivation up to the end of 96 h (30 relative % for the CH_4 conversion and 22 relative % for CO_2 conversion). This can be
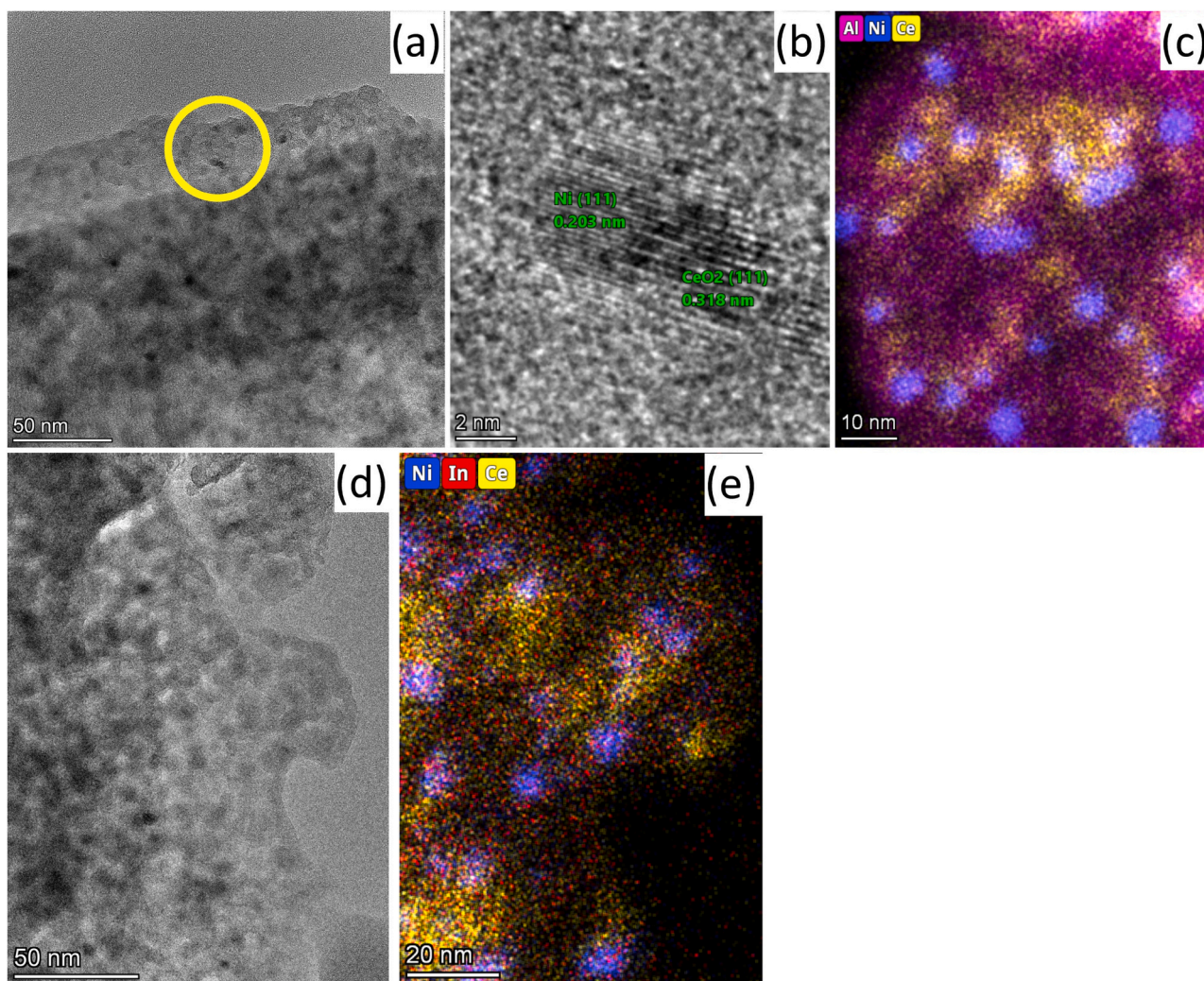
Fig. 9. Results of TEM investigations of catalysts used in the short DRM test. a) TEM image of Ni-CeAl; b) HRTEM of the circled area of Ni-CeAl; c) STEM-EDS elemental maps of Al, Ni, Ce over Ni-CeAl; d) TEM image of NiIn-CeAl and e) STEM-EDS elemental maps of Ni, In, Ce over NiIn-CeAl.
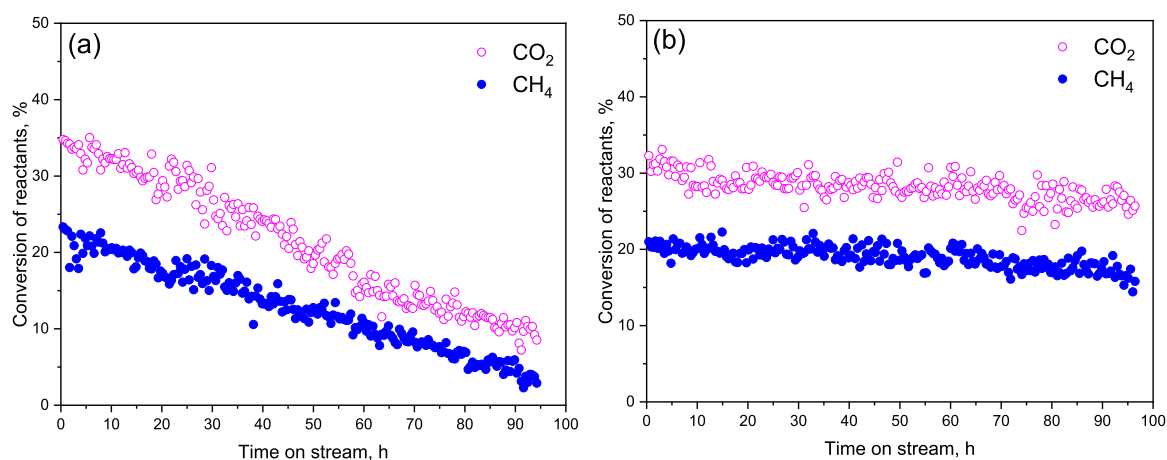
Fig. 10. Methane and CO_2 conversion curves during the longevity DRM tests over a) Ni-CeAl and b) NiIn-CeAl samples. The H_2/CO ratio was constant and 0.62 for Ni-CeAl and 0.52 for NiIn-CeAl thorough the experiments. Conditions: after reduction at 750 °C/1 h cooling to T = 675 °C in N_2, then DRM with $CH_4:CO_2 = 1:1$ mixture, 210 L/h/g_{cat}, TOS= 96 h.

considered as a significantly higher stability under these demanding conditions. As the CO_2/CH_4 ratio was higher (2.1) and the H_2/CO ratio was lower (0.52) than in the case of the In-free sample, we can point out

that indium increases the rates of all CO_2 converting side reactions, as was already observed in the same type samples but produced by deposition precipitation method [14], but these apparently lead to a longer

catalyst lifetime beside an acceptably stable CH_4 dissociation rate up to 4 days timeframe. All in all, the 4 day-long stability tests revealed the primacy of NiIn-CeAl catalyst when thinking of perspective catalyst formulations for more realistic conditions, when long catalyst lifetime is a must. The unpromoted counterpart, although it is perfect within a short range, loses the ability to produce CO-rich synthesis gas after some time.

The presence and the oxidation ability of any deposited carbon was determined by TPO measurements after the longevity tests (Fig. S2). The TPO curve quantification revealed 0.16 wt% carbon for NiIn-CeAl sample and ten times more, 1.5 wt% carbon in the case of Ni-CeAl catalyst. The values are not high, but still, Ni-CeAl sample deactivated at the end of the long test and the bimetallic catalyst remained active. The carbon deposits could fully deactivate the catalyst only if present as (graphitic) carbon layers over the nickel particles. The oxidation of graphitic carbon in close contact with the metal can be detected above 450–500 °C depending on the support. Ceria is a good oxidation co-catalyst, this is why the oxidation of carbon deposited over these samples are expected to appear at lower temperatures. Indeed, the main TPO peak shown in Fig S2 for the Ni-CeAl had two components: one with a maximum at 465 °C and a shoulder at 570 °C. The higher temperature definitely refers to a massive graphitic type of coke, while the one at lower temperature may be finer, partially amorphous but in contact with the metal particles and the support as well. The bimetallic NiIn-CeAl catalyst produced insignificant amount of deposited carbon that appeared just above the signal noise at 650 °C suggesting some graphitic type of carbon.

The morphology of the spent samples was further studied by TEM. Fig. 11 a-c show the images of used Ni-CeAl. Particle size of Ni on the support appeared to be still small, (see the TEM image in Fig. 11a), around 7 nm. Carbon coverage around the supported Ni particles could not be observed, although the TPO suggested two type of carbon with different oxidation properties. Beside the catalyst grain in Fig. 11a, a separated carbon tube with metallic Ni particle inside was also observable. According to the enlarged HRTEM image in Fig. 11b, the ~39 nm sized elongated particle is wrapped by several layers of graphitic carbon and a long tail of multiwalled 150 nm long carbon nanotube. Such structures were seen at other places of the TEM specimen as shown in Fig. 11c. Thus, based on these TEM images we can conclude that particle size sintering and carbon coverage was the cause of catalyst deactivation in the case of unpromoted Ni-CeAl sample during the 4 day-longevity tests. The overoxidation of Ni caused by the H_2O formation could be another reason of deactivation, because the amount of deposited carbon was not too high, but we could not find any proof for that.

The TEM results of spent NiIn-CeAl after the long test are collected in Fig. 12a-d. The general view of this sample is again similar to that of Ni-

CeAl catalyst, where large, aggregated Ni particles showing strong sintering over the support were not seen at all. After 96 h of TOS, the Ni(In) parts are still nicely distributed among the CeO_x-Al_2O_3 matrix (Fig. 12a). Carbon deposit over the catalyst aggregates was not detected, but individual thin carbon nanotubes with diameter under 20 nm were found at a few places. Fig. 12b shows an unusual big group of such nanotubes. These thin, fine tubes enlarged in Fig. 12.c-d contained metal particles with spacings corresponding to Ni(111) lattice. Their Ni size was maximum 15 nm, with an exception that is shown in Fig. 12c being 36 nm in its widest dimension. The most important observation is that these Ni(In) particles were not completely covered by carbon layers in contrast to the ones in Ni-CeAl catalyst: at one end they were almost free of carbonaceous layers suggesting that they have still active sites to carry on the reaction. This must be due to the presence of indium sites along the Ni surface that can be partially oxidized by H_2O or CO_2 than reduced by H_2 or CO, providing active oxygen or OH species thus keeping Ni clean and active. The portion of indium oxide species that was present in the mixed oxide phase in contact with the metallic particles could serve as atomic glue and prevent Ni from significant size increase. Moreover, this surrounding In-oxide buried in the CeO_2-Al_2O_3 matrix promotes CO_2 activation that can again boost oxygen or OH transport to remove surface CH_x species from Ni. The little deactivation observed must be attributed to some Ni sintering, as large Ni particles as in Ni-CeAl catalyst were not observed. The highly positive effect of 0.25 wt% indium promotion beside the strong Ni-CeO_2 interaction and the extended Ni/CeO_2 interface is clearly reflected by the morphological and catalytic stability of NiIn-CeAl sample.

3.6. The influence of impregnation method on the Ni-In-CeO₂ interaction in alumina matrix

Our previous publication about Ni and $NiIn/CeO_2$-Al_2O_3 catalysts having the same metal loadings but prepared by deposition precipitation method [14] reported a higher catalytic activity in the 650 °C tests but higher coking tendency as well than what were experienced in the present case. The largest difference between the samples of the two synthesis (DP versus impregnation) routes was the nickel-support interaction being much stronger in the case of impregnation. This resulted in a NiO-(In_2O_3)-CeO_2-Al_2O_3 mixed oxide with a vast majority of aluminate after calcination. TPR analysis revealed that the NiO species were reduced to the metallic state only above 600 °C in the case of impregnation method, regardless of whether indium promoter was present or not. The resulting particle size was definitely lower than with the DP method, but an exact particle size distribution could not be determined. According to the DRIFTS results, indium was alloyed with nickel and the bimetallic particles were partly oxidized by CO_2 but did
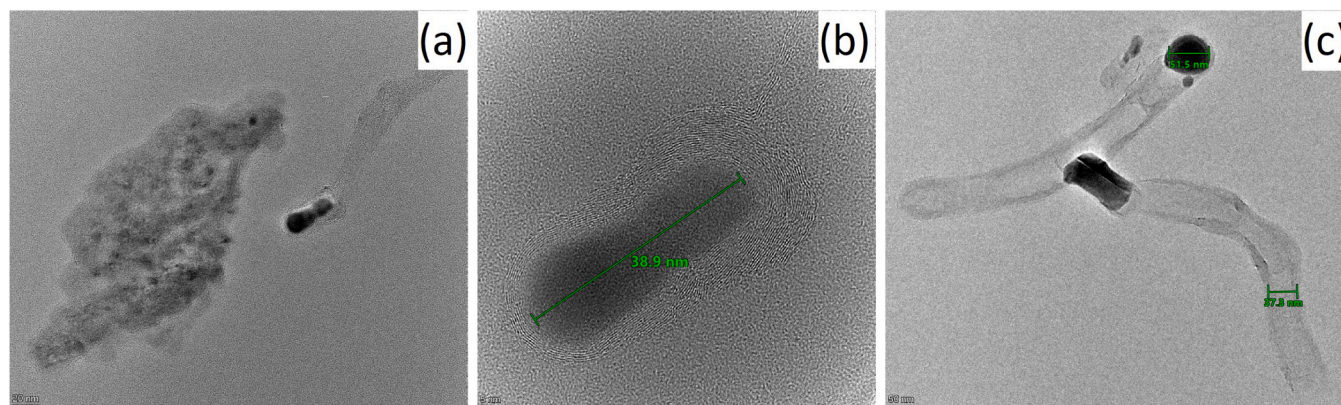
Fig. 11. Results of TEM investigations of Ni-CeAl catalyst used in the longevity DRM test. a) a representative TEM image with a catalyst grain and a carbon nanotube with Ni particle inside; b) HRTEM image of the same single nanotube with the encapsulated large Ni particle; c) TEM image of other carbon nanotubes with Ni particles inside.
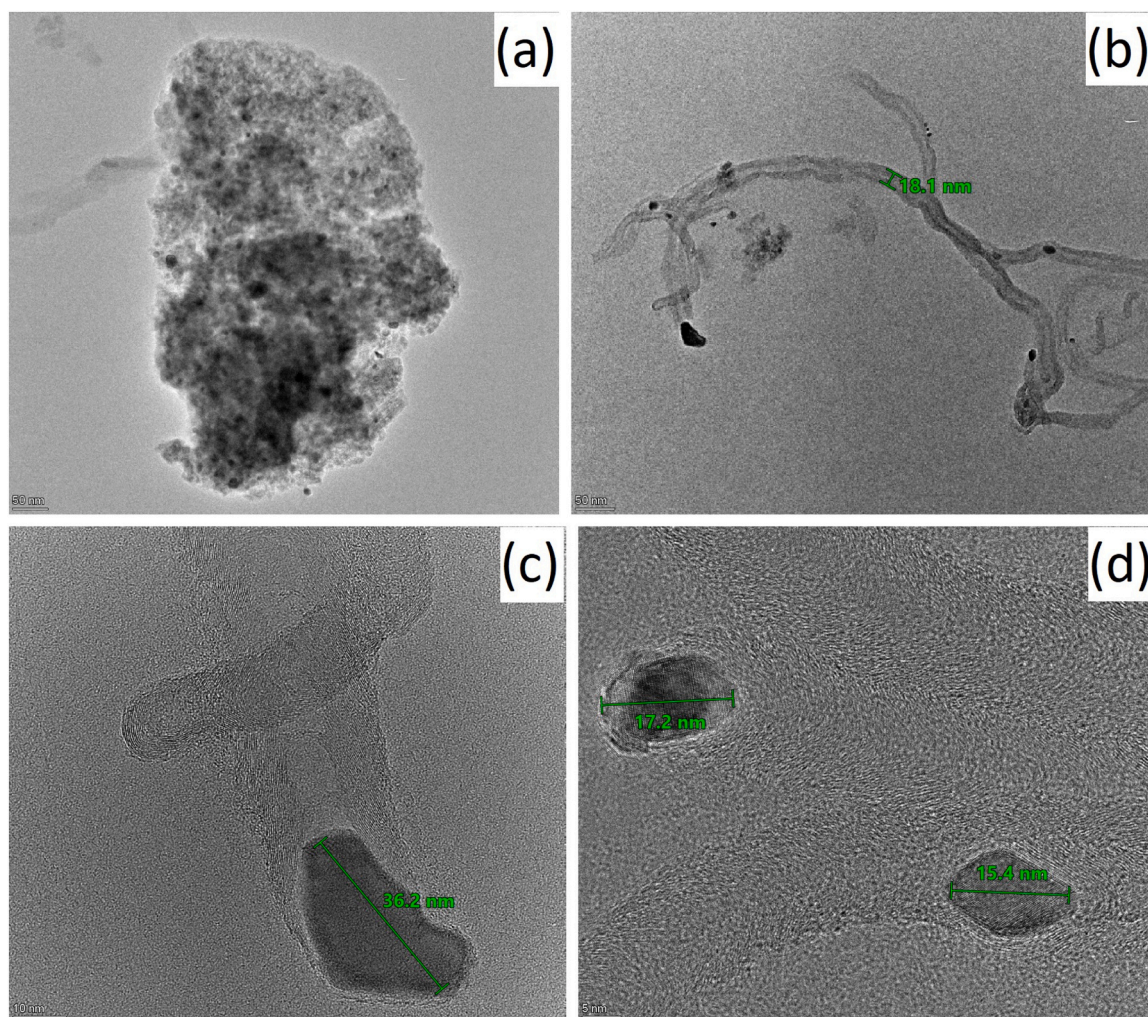
Fig. 12. Results of TEM investigations of NiIn-CeAl catalyst used in the longevity DRM test. a) a representative TEM image of a catalyst grain; b) a group of separated thin carbon nanotubes with Ni particles inside or at the end of the tube; c) HRTEM image of the same nanotubes with Ni(In) particle at the end; d) HRTEM image of smaller Ni(In) particles inside or at the end of herringbone carbon nanotubes.

not dissociate CO – in contrast to the monometallic Ni catalyst. Due to the extended, intimate Ni-CeO$_2$ interface of small Ni particles and the CeO$_2$ islands, stable activity could be achieved at 650 °C without coke formation, but indium lowered the CH$_4$ dissociation ability (CH$_4$ conversion was less). At higher temperature (675 °C), the dominance of the promoted sample was eye-catching as it was stable and active for 4 days, while the In-free counterpart slowly lost its catalytic activity due to carbon coverage and sintering of nickel. The intrinsic RWGS activity of In-containing catalyst was observed under these conditions and this is the parameter that helps to keep nickel sites clean and available. As during DRM reaction water is always present, it can oxidize metallic indium (in NiIn alloy) forming InO$_x$H$_y$ or InO$_x$ [36,37]. On the other side, indium-oxide can be reduced by H$_2$ [38,39] or CO [40], and on the partially reduced sites CO$_2$ dissociation can happen [41].

The two types of catalytic experiments underscore the importance of long-term catalyst testing and highlight the positive contribution of indium in Ni-containing dry reforming catalysts. In general, higher Ni size stability, resistance against sintering, less coke deposition are the positive effects of indium occluded inside the CeO$_2$-Al$_2$O$_3$ matrix and alloyed with nickel.

Based on our experience with other indium-loaded samples, the Ni-In interaction greatly depends on the support composition. The effect observed with mixed CeO$_2$-Al$_2$O$_3$ carriers is influenced by the preparation method, i.e. by the position of the nickel particles (mainly in the

pores or not), their dispersion and their interaction with the CeO$_2$ component. It appears that the dual role of indium as a promoting component in the oxide support and in the metal component is a dynamically changing function.

4. Conclusions

In the present work, the structural and dry reforming properties of a Ni/CeO$_2$-Al$_2$O$_3$ catalyst and its 0.25% In-promoted NiIn/CeO$_2$-Al$_2$O$_3$ counterpart were investigated and compared. The catalyst synthesis was carried out by impregnation in two steps: first, the mixed support was prepared (commercial alumina impregnated with Ce nitrate) and calcined, then the Ni and In precursors were co-impregnated onto the mixed support and another calcination step was performed. The samples were analyzed by various structural characterization methods, while the dry reforming activity of methane was tested in a thin plug flow reactor at 650 °C for 6 h (short tests) and at 675 °C for 4 days (longevity tests) in a wider reactor tube, i.e., with a different catalyst bed aspect ratio, each in conjunction with coke quantification.

TPR analysis revealed NiO species very strongly interacting with the support that formed small metal particles upon 750 °C reduction treatment, but some NiO must have remained in an oxidic state as Ni aluminate near the support surface. The XPS results indicated that indium increased the amount of metallic nickel through its close contact or

alloy formation with Ni and decreased the surface concentration of Ce^{3+}. The Ni particle size of the samples was small and was still about 5 nm after the short catalytic reactions. The formation of bimetallic NiIn particles was demonstrated by DRIFTS experiments. Some type of surface segregation, likely due to partial oxidation of In, was detected by DRIFTS-DRM and DRIFTS-CO_2 measurements, while CO was not dissociated across the bimetallic surface according to DRIFTS-CO studies. In the short DRM tests at 650 °C, the catalysts were very stable and exhibited almost no surface carbon, but the activity was lower for the In-promoted sample. Under a longer timescale at 675 °C and using different reactor geometry, the catalyst without indium exhibited a continuous loss of activity, while the bimetallic sample lasted to the end of the test with only a small degree of deactivation. The deactivation of the monometallic catalyst can be explained by the moderate coking covering the nickel sites and partly by sintering. In the bimetallic catalyst, beside some sintering, the nickel could remain free of carbon and active by the minuscule In-promotion that had such a tremendous effect.

We have already noted that such a small amount of indium must have a significant effect when alloyed with nickel, but the chance for such alloy formation is even smaller if indium(oxide) penetrates deeply into the structure of the oxide matrix and is held there with a strong interaction. However, if there is also a nickel component in the porous structure, reduction pretreatment can cause alloy formation of both components. The impregnation method seems to manifest this situation.

CRediT authorship contribution statement

Anita Horváth: Conceptualization, Investigation, Writing – original draft, Writing – review & editing. **Miklós Németh**: Investigation, Methodology, Visualization, Writing – original draft. **Andrea Beck**: Methodology, Writing – review & editing. **György Sáfrán**: Investigation. **Valeria La Parola**: Conceptualization, Investigation, Writing – original draft. **Leonarda Francesca Liotta**: Investigation, Visualization. **Gregor Žerjav**: Investigation, Visualization. **Matevž Roškarič**: Investigation. **Albin Pintar**: Writing - review & editing, Supervision.

Declaration of Competing Interest

The authors declare that they have no known competing financial interests or personal relationships that could have appeared to influence the work reported in this paper.

Data availability

Data will be made available on request.

Appendix A. Supporting information

Supplementary data associated with this article can be found in the online version at doi:10.1016/j.apcata.2023.119495.

References

[1] J.R. Rostrup-Nielsen, J. Sehested, J.K. Nørskov, Advances in Catalysis, Academic Press, 2002, pp. 65–139.

[2] A. Erdőhelyi, Catalytic reaction of carbon dioxide with methane on supported noble metal catalysts, Catalysts 11 (2021) 159.

[3] M.A. Vasiliades, C.M. Damaskinos, K.K. Kyprianou, M. Kollia, A.M. Efstathiou, The effect of Pt on the carbon pathways in the dry reforming of methane over Ni-Pt/Ce0.8Pr0.2O2-δ catalyst, Catal. Today 355 (2020) 788–803.

[4] G. Zhang, J. Liu, Y. Xu, Y. Sun, A review of CH4-CO2 reforming to synthesis gas over Ni-based catalysts in recent years (2010-2017), Int. J. Hydrog. Energy 43 (2018) 15030–15054.

[5] L. Wang, F. Wang, Design strategy, synthesis, and mechanism of Ni catalysts for methane dry reforming reaction: recent advances and future perspectives, Energy Fuels 36 (2022) 5594–5621.

[6] Y. Shi, L. Wang, M. Wu, F. Wang, Order-of-magnitude increase in rate of methane dry reforming over Ni/CeO2-SiC catalysts by microwave catalysis, Appl. Catal. B: Environ. 337 (2023), 122927.

[7] K. Han, Y. Wang, S. Wang, Q. Liu, Z. Deng, F. Wang, Narrowing band gap energy of CeO2 in (Ni/CeO2)@SiO2 catalyst for photothermal methane dry reforming, Chem. Eng. J. 421 (2021), 129989.

[8] D. Pakhare, J. Spivey, A review of dry (CO2) reforming of methane over noble metal catalysts, Chem. Soc. Rev. 43 (2014) 7813–7837.

[9] K. Han, S. Wang, Q. Liu, F. Wang, Optimizing the Ni/Cu Ratio in Ni–Cu nanoparticle catalysts for methane dry reforming, ACS Appl. Nano Mater. 4 (2021) 5340–5348.

[10] K. Han, S. Wang, N. Hu, W. Shi, F. Wang, Alloying Ni–Cu nanoparticles encapsulated in SiO2 nanospheres for synergistic catalysts in CO2 reforming with methane reaction, ACS Appl. Mater. Interfaces 14 (2022) 23487–23495.

[11] J. Károlyi, M. Németh, C. Evangelisti, G. Sáfrán, Z. Schay, A. Horváth, F. Somodi, Carbon dioxide reforming of methane over Ni–In/SiO2 catalyst without coke formation, J. Ind. Eng. Chem. 58 (2018) 189–201.

[12] M. Németh, G. Sáfrán, A. Horváth, F. Somodi, Hindered methane decomposition on a coke-resistant Ni-In/SiO2 dry reforming catalyst, Catal. Commun. 118 (2019) 56–59.

[13] M. Németh, F. Somodi, A. Horváth, Interaction between CO and a coke-resistant NiIn/SiO2 methane dry reforming catalyst: a DRIFTS and CO pulse study, J. Phys. Chem. C. 123 (2019) 27509–27518.

[14] A. Horváth, M. Németh, A. Beck, B. Maróti, G. Sáfrán, G. Pantaleo, L.F. Liotta, A. M. Venezia, V. La Parola, Strong impact of indium promoter on Ni/Al2O3 and Ni/CeO2-Al2O3 catalysts used in dry reforming of methane, Appl. Catal. A: Gen. 621 (2021), 118174.

[15] J.B. Wang, Y.-L. Tai, W.-P. Dow, T.-J. Huang, Study of ceria-supported nickel catalyst and effect of yttria doping on carbon dioxide reforming of methane, Appl. Catal., A 218 (2001) 69–79.

[16] P. Djinović, A. Pintar, Stable and selective syngas production from dry CH4-CO2 streams over supported bimetallic transition metal catalysts, Appl. Catal. B: Environ. 206 (2017) 675–682.

[17] K. Han, S. Xu, Y. Wang, S. Wang, L. Zhao, J. Kambonde, H. Yu, W. Shi, F. Wang, Confining Ni and ceria in silica shell as synergistic multifunctional catalyst for methane dry reforming reaction, J. Power Sources 506 (2021), 230232.

[18] A. Pardo, S. Feliú, M.C. Merino, R. Arrabal, E. Matykina, The effect of cerium and lanthanum surface treatments on early stages of oxidation of A361 aluminium alloy at high temperature, Appl. Surf. Sci. 254 (2007) 586–595.

[19] J.M. Rynkowski, T. Paryjczak, A. Lewicki, M.I. Szynkowska, T.P. Maniecki, W. K. Jóźwiak, React. Kinet. Catal. Lett. 71 (2000) 55–64.

[20] H. Wu, G. Pantaleo, V. La Parola, A.M. Venezia, X. Collard, C. Aprile, L.F. Liotta, Bi- and trimetallic Ni catalysts over Al2O3 and Al2O3-MO (M = Ce or Mg) oxides for methane dry reforming: Au and Pt additive effects, Appl. Catal., B 156– 157 (2014) 350–361.

[21] J. Lu, Y. Lei, G. Wan, Z. Mei, J. Yu, Y. Zhao, S. He, Y. Luo, Weakening the metal-support strong interaction to enhance catalytic performances of alumina supported Ni-based catalysts for producing hydrogen, Appl. Catal., B 263 (2020) 118177.

[22] M.K. Gnanamani, G. Jacobs, W.D. Shafer, S.D. Hopps, B.H. Davis, Dehydration of pentanediol over CeO2, CeO2-Ga2O3, and CeO2-In2O3, ChemistrySelect 2 (2017) 4150–4156.

[23] C. Yang, H. Li, A. Zhang, Z. Sun, X. Zhang, S. Zhang, L. Jin, Z. Song, Effect of indium addition on the low-temperature selective catalytic reduction of NO (x) by NH(3) over MnCeO (x) catalysts: the promotion effect and mechanism, ACS Omega 7 (2022) 6381–6392.

[24] Y.I. Choi, S.K. Kim, S.W. Lee, Y. Sohn, Metallic indium spheres by the anaerobic ethanol oxidation of indium oxide, J. Alloy. Compd. 687 (2016) 611–615.

[25] P. Burroughs, A. Hamnett, A.F. Orchard, G. Thornton, Satellite structure in the X-ray photoelectron spectra of some binary and mixed oxides of lanthanum and cerium, J. Chem. Soc., Dalton Trans. (1976) 1686–1698.

[26] G. Poncelet, M.A. Centeno, R. Molina, Characterization of reduced α-alumina-supported nickel catalysts by spectroscopic and chemisorption measurements, Appl. Catal., A 288 (2005) 232–242.

[27] R.G. Tobin, S. Chiang, P.A. Thiel, P.L. Richards, The C═O stretching vibration of CO on Ni(100) by infrared emission spectroscopy, Surf. Sci. 140 (1984) 393–399.

[28] A. Bandara, S. Dobashi, J. Kubota, K. Onda, A. Wada, K. Domen, C. Hirose, S. S. Kano, Adsorption of CO and NO on surface studied by infrared-visible sum frequency generation spectroscopy, Surf. Sci. 387 (1997) 312–319.

[29] M. Agnelli, H.M. Swaan, C. Marquez-Alvarez, G.A. Martin, C. Mirodatos, CO hydrogenation on a nickel catalyst, J. Catal. 175 (1998) 117–128.

[30] M. Mihaylov, K. Hadjiivanov, H. Knözinger, Catal. Lett. 76 (2001) 59–63.

[31] A. Cárdenas-Arenas, A. Quindimil, A. Davó-Quiñonero, E. Bailón-García, D. Lozano-Castelló, U. De-La-Torre, B. Pereda-Ayo, J.A. González-Marcos, J. R. González-Velasco, A. Bueno-López, Isotopic and in situ DRIFTS study of the CO_2 methanation mechanism using Ni/CeO2 and Ni/Al2O3 catalysts, Appl. Catal. B: Environ. 265 (2020), 118538.

[32] U. Oemar, Z. Bian, K. Hidajat, S. Kawi, Sulfur resistant LaxCe1−xNi0.5Cu0.5O3catalysts for an ultra-high temperature water gas shift reaction, Catal. Sci. Technol. 6 (2016) 6569–6580.

[33] W. Wang, Y. Zhang, Z. Wang, J. Yan, Q. Ge, C. Liu, Reverse water gas shift over In 2 O 3 –CeO 2 catalysts, Catal. Today 259 (2016) 402–408.

[34] J. Zhang, H. Wang, A.K. Dalai, Development of stable bimetallic catalysts for carbon dioxide reforming of methane, J. Catal. 249 (2007) 300–310.

[35] W. Luhui, Z. Shaoxing, L.I.U. Yuan, Reverse water gas shift reaction over Co-precipitated Ni-CeO2 catalysts, J. Rare Earths 26 (2008) 66–70.

[36] Z.M. Detweiler, S.M. Wulfsberg, M.G. Frith, A.B. Bocarsly, S.L. Bernasek, The oxidation and surface speciation of indium and indium oxides exposed to atmospheric oxidants, Surf. Sci. 648 (2016) 188–195.

[37] K. Otsuka, A. Mito, S. Takenaka, I. Yamanaka, Production of hydrogen from methane without CO_2-emission mediated by indium oxide and iron oxide, Int. J. Hydrog. Energy 26 (2001) 191–194.

[38] M.S. Frei, M. Capdevila-Cortada, R. García-Muelas, C. Mondelli, N. López, J. A. Stewart, D. Curulla Ferré, J. Pérez-Ramírez, Mechanism and microkinetics of methanol synthesis via CO_2 hydrogenation on indium oxide, J. Catal. 361 (2018) 313–321.

[39] A.I. Serykh, Low-dimensional indium oxo-species on the surface of In2O3/ Al2O3catalytic material: the sites of dissociative adsorption of hydrogen, J. Phys. Chem. C. 120 (2016) 21436–21440.

[40] K. Otsuka, T. Yasui, A. Morikawa, The decomposition of water on the CO- or H2-reduced indium oxide, Bull. Chem. Soc. Jpn. 55 (1982) 1768–1771.

[41] O. Martin, A.J. Martín, C. Mondelli, S. Mitchell, T.F. Segawa, R. Hauert, C. Drouilly, D. Curulla-Ferré, J. Pérez-Ramírez, Indium oxide as a superior catalyst for methanol synthesis by CO_2 hydrogenation, Angew. Chem. Int. Ed. 55 (2016) 6261–6265.